AJNR

Histopathologic and Immunohistochemical Comparison of Human, Rabbit, and Swine Aneurysms Embolized with Platinum Coils

Daying Dai, Yong Hong Ding, Mark A. Danielson, Ramanathan Kadirvel, Debra A. Lewis, Harry J. Cloft and David F. Kallmes

AJNR Am J Neuroradiol 2005, 26 (10) 2560-2568
http://www.ajnr.org/content/26/10/2560

AJNR Am J Neuroradiol 26:2560–2568, November/December 2005

Histopathologic and Immunohistochemical Comparison of Human, Rabbit, and Swine Aneurysms Embolized with Platinum Coils

Daying Dai, Yong Hong Ding, Mark A. Danielson, Ramanathan Kadirvel, Debra A. Lewis, Harry J. Cloft, and David F. Kallmes

BACKGROUND AND PURPOSE: **The purpose of this study was to clarify the cellular mechanisms of aneurysmal healing by comparing histologic and immunohistochemical findings in experimental rabbit and swine aneurysms to a human aneurysm embolized with platinum coils.**

METHODS: **Swine sidewall aneurysms ($n = 5$, harvested at 12 weeks) and elastase-induced rabbit aneurysms ($n = 6$, harvested at 24 weeks) were created and embolized. A single human aneurysm, embolized 6 years before death, was harvested following autopsy. All specimens were processed by using a modified paraffin embedding technique. Tissue was sectioned and stained with hematoxylin and eosin and Masson trichrome. Immunohistochemistry and immunofluorescence were performed with multiple antibodies, including alpha smooth muscle actin, myosin heavy chain, desmin, vimentin, and CD31.**

RESULTS: **The human aneurysm's dome was filled with loose, hypocellular, amorphous tissue. The aneurysm's neck was completely covered with a thin layer of hypocellular tissue. Collagen and myofibroblasts were sparse in both the dome and neck. Rabbit aneurysms' domes were also filled with a loose, hypocellular tissue, amorphous matrix. In 5 of 6 aneurysms, a thin layer of hypocellular tissue ran along the neck. Collagen and myofibroblasts were sparse in the dome. Swine aneurysms were filled with densely infiltrated tissue, including chronic inflammatory tissue and extensive, attenuated collagen fiber bundles associated with myofibroblasts. Thick layers of myofibroblasts entirely bridged the necks.**

CONCLUSIONS: **Absence of collagen deposition and scant myofibroblastic reaction to platinum coil embolization are seen in the rabbit model but not in swine aneurysms. The elastase-induced aneurysm model in rabbits is more suitable than sidewall swine aneurysms for testing of modified devices aimed at improving intra-aneurysmal fibrosis.**

Platinum coils have proved to be a valuable alternative to open surgical clipping for the treatment of intracranial aneurysms. However, limited histopathologic data in coil-embolized aneurysms in humans (1–6) and animal experiment studies (7–11) have suggested that platinum coils are biologically inert and fail to elicit a fibrotic response. These findings have prompted numerous investigators to explore coil modifications aimed at increasing the coil's biologic activity (12–23).

Advancing the efficacy of endovascular devices relies heavily on preclinical testing in animal models. An ideal animal model of human saccular aneurysms would mimic human histomorphologic and hemodynamic features, as well as simulate the human cellular and molecular milieu. Previously developed animal models, including surgically created aneurysms in canines and swine, have been widely used for preclinical testing of endovascular devices in the past decade (7, 12, 16–19, 24–28). The use of surgically created, vein patch aneurysms, however, becomes questionable in the age of biologic modification, because the presence of disrupted arterial walls and suture lines yields unknown effects on the biology of the models. More recently, elastase-induced aneurysms in rabbits have been proposed as a useful preclinical tool for device development (9, 20–23, 29–32). Our previously pub-

Received February 16, 2005; accepted after revision May 18.

From the Neuroradiology Research Laboratory, Department of Radiology, Mayo Clinic, Rochester, MN.

This work was supported by research grant NS42646 from the National Institutes of Health.

These data were presented at the 43rd annual meeting of the American Society of Neuroradiology Meeting, Toronto, Ontario, Canada, May 21–27, 2005.

Address correspondence to David F. Kallmes, MD, Mayo Clinic, 200 First Street, SW, Rochester, MN 55905.

lished data (29, 30) have shown these model aneurysms are similar to that of human aneurysms in size and shape, and, left untreated, aneurysms remain patent reliably for as long as 2 years (Y. H. Ding et al, unpublished data, 2005). Furthermore, because these experimental aneurysms occur at a prominent curve along the brachiocephalic artery and are close to the aorotic root, the aneurysm neck is subject to high shear stress (33–35), similar to that noted in ophthalmic aneurysms in humans (30). In addition, the wall of this model simulates human aneurysms with the internal elastic lamina markedly diminished or absent (29, 36). Finally, model creation is done without the need for sutures along the aneurysm neck.

Relatively little is known about the histopathologic differences and cellular and biologic reactions to coil embolization among species, including human aneurysms. In addition, there currently exists no reliable technique for detailed histopathologic study of aneurysms treated with endovascular coils. The presence of metal precludes standard processing methods. Thus, few previous reports have applied any advanced histologic techniques such as immunohistochemistry or immunofluorescence to explore the cellular and biologic reaction induced by coil embolization. As a result, the biologic response to an implanted device is clouded and the understanding of the healing response to coils remains poor.

In the present study, a modified paraffin-embedding technique for processing coil-bearing tissue was used to compare the long-term histopathologic and immunohistochemical findings in rabbit and swine aneurysms. These findings were compared with those in a single human aneurysm, in an attempt to further clarify the cellular mechanisms of healing in these species.

Materials and Methods

Rabbit Saccular Aneurysm Model

Elastase-induced, saccular aneurysms were created in New Zealand white rabbits (body weight 3–4 kg) by using the rabbit elastase model. The Institutional Animal Care and Use Committee at our institution approved all procedures before the start of the study. The detailed procedures for aneurysm creation have been described in depth elsewhere (29). In brief, anesthesia was induced with an intramuscular injection of ketamine, xylazine, and acepromazine (75, 5, and 1 mg/kg, respectively). Using sterile technique, the right common carotid artery (CCA) was exposed and ligated distally. A 1–2-mm beveled arteriotomy was made, and a 5F vascular sheath was advanced retrograde in the right CCA to a point approximately 3 cm cephalad to the origin of right CCA. A 3F Fogarty balloon was advanced through the sheath to the level of the origin of the right CCA with fluoroscopic guidance and was inflated with iodinated contrast material. Porcine elastase (Worthington Biochemical Corporation, Lakewood, NJ) was incubated within the lumen of the common carotid above the inflated balloon for 20 minutes, after which the catheter, balloon, and sheath were removed. The right CCA was ligated below the sheath entry site, and the incision was sutured.

Rabbit Aneurysm Embolization Procedure

Aneurysms were permitted to mature for at least 21 days following creation. The anesthesia as described for aneurysm creation was employed for this procedure. By using a sterile technique, surgical exposure of the right common femoral artery (CFA) was performed. The artery was ligated distally by using 4–0 silk suture, and a 22-gauge angiocatheter was advanced retrograde into the artery. A guidewire (0.018 inches) was passed through the angiocatheter followed by placement of a 5F vascular sheath. Heparin (100 U/kg) was administered intravenously. A 5F catheter was advanced into the brachiocephalic artery. By using the coaxial technique, with continuous heparinized saline flush, a 2-marker microcatheter was advanced into the aneurysm cavity. The size of the aneurysm cavity was assessed by direct comparison to radiopaque sizing devices during digital subtraction angiography (DSA). Aneurysms were embolized with platinum coils as described elsewhere (9). Aneurysm cavities were densely packed in all cases. Following embolization, a final control DSA was performed. The catheters and sheath were removed, the femoral artery was ligated, and the incision was closed.

Aneurysms were harvested at 24 weeks ($n = 6$). At the time of sacrifice, the subjects were deeply anesthetized as in aneurysms creation and embolization and then were euthanized with a lethal injection of pentobarbital. The chest cavity was opened, and the mediastinum was dissected; the coil-embolized aneurysm was then exposed and dissected free from surrounding tissues. Specimens were fixed in 10% neutral buffered formalin for a minimum of 24 hours. The gross appearance of the neck of the aneurysm was carefully examined by using a dissecting microscope and photographed.

Swine Sidewall Aneurysm Model

Sidewall aneurysms were created in domestic swine (body weight 30–40 kg) by using the methods of German and Black (37). In brief, anesthesia was achieved by intramuscular injection of telazol (5 mg/kg) and xylazine (1.0 mg/kg) and maintained by means of inhaled isofluorane gas 1%–3%. Employing a sterile technique, a neck midline incision (~10 cm) was made. The right external jugular vein was exposed and isolated and a pair of 4-cm lengths of vein were harvested and placed in sterile saline. The right carotid artery was exposed, cleaned of adventitia, and clamped with DeBakey vascular clamps proximally and distally. After achieving stasis in this isolated segment, an arteriotomy (~7 mm diameter) was made and an end-to-side anastomosis (vein to artery) was performed by using 7–0 prolene with interrupted sutures. When the surgeon was satisfied with the anastomosis, the proximal clamp was released and blood flow was re-established through the artery and to the aneurysm. The resulting aneurysm was then embolized with platinum coils.

Swine Embolization Procedure

Because the swine model has strong tendency for spontaneous thrombosis (18), once the aneurysm was created, it was immediately embolized. A cutdown was performed to gain percutaneous access to the right CFA. A 6F sheath was placed and connected to continuous heparinized saline flush. Systemic anticoagulation was achieved with intravenous heparin (150U/kg bolus). A 6F guide catheter was placed over an angled guidewire into the proximal right CCA. A microcatheter was then inserted coaxially through the guide catheter into the midright CCA. DSA was performed with injection of 5 mL of iodinated contrast medium (Omnipaque 300; Nycomed, Princeton, NJ). External sizing markers were used to determine the dimensions of the aneurysm. A platinum coil was placed into the aneurysm through a microcatheter as described elsewhere by our group (9). Additional coils were placed until attenuated packing was achieved. In certain cases, balloon assistance was used to facilitate coil placement. After both

aneurysms were created and embolized, the catheters and sheaths were removed and the incisions were closed.

Aneurysms were harvested at 12 weeks ($n = 5$). At time of sacrifice, the subjects were deeply anesthetized as above and then were euthanized with a lethal injection of pentobarbital. The CCAs, including the aneurysm with coils, were dissected from around tissue, removed, and placed in 10% neutral buffered formalin for a minimum of 24 hours. The gross appearance of the neck of the aneurysm was carefully examined and photographed.

Human Aneurysm

The single human aneurysm was from a 71-year-old man who died of a ruptured anterior communicating artery aneurysm. Six years before his death (1998), he had been diagnosed with a vertebrobasilar aneurysm. The aneurysm was embolized with Guglielmi detachable coils (GDCs; Boston Scientific, Natick, MA) at that time. Upon his death, an autopsy limited to the brain was performed. The coiled aneurysm at the junction of the vertebral and basilar arteries was carefully harvested for study.

Histology

A single researcher (D.D.) performed all the histologic procedures. Two experienced observers (D.D. and D.F.K.) reviewed and interpreted all histologic slides.

Tissue-Processing Procedure

All the fixed aneurysms (rabbit, swine, and human) were dehydrated in an ascending series of ethanol, cleared in xylene, and embedded in paraffin. By using an Isomet low-speed saw with a series 15HC diamond blade, the aneurysms were sectioned at 1000-μm intervals through the portion bearing metallic coils in a coronal orientation, allowing long-axis sectioning of the aneurysm neck. Under a dissecting microscope, the metallic coil fragments were carefully removed from the 1000-μm sections. Following removal of all coil fragments, the sections were re-embedded in paraffin blocks. These blocks were sectioned employing a microtome (Leica Microsystems, Nussloch, Germany, model RM2165) with disposable blades at 5–6-μm intervals. Sections were then floated on a water-bath at 42°C to remove the wrinkles, then mounted on Superfrost Plus slides (Fisher Scientific, Pittsburgh, PA) and dried overnight in an oven at 37°C.

Hematoxylin and Eosin

At least 2 sections from each block were stained with hematoxylin and eosin (H&E) contrast for conventional histopathologic evaluation.

Masson Trichrome Stain

Serial sections were stained with Masson Trichrome. The slides were deparaffinized and hydrated in distilled water and were then placed in Bouin's solution for 30 minutes in a 56°C water bath. They were rinsed in running tap water until the sections were colorless. Then sections were stained in filtered Weigert iron hematoxylin working solution for 10 minutes, followed by a tap water rinse for 5 minutes. After rinsing the sections in distilled water, they were stained in Biebrich scarlet acid fuchsin for 4 minutes and then rinsed in distilled water. The rinsed sections were placed in phosphomolybdic-phosphotungstic acid working solution for 12 minutes and then placed in aniline blue solution for 20 minutes. Finally, after the slides were rinsed in distilled water, they were placed in 1% acetic acid for 4 minutes and then dehydrated through alcohols, cleared in xylene, and mounted with EZ-Mount (Thermo Shandon, Pittsburgh, PA).

Immunohistochemistry

The Vectastain Elite ABC system (Vector Laboratories, Burlingame, CA) was used for immunohistochemistry (IHC). Sections were dried at 56°C for 1–2 hours, deparaffinized and hydrated in water, and then incubated with hydrogen peroxide (0.3% in distilled water) for 20 minutes. Sections were pretreated with 0.1 mol/L citric acid buffer in a microwave for 15 minutes. Slides were left to cool at room temperature for 30 minutes before being rinsed in phosphate-buffered saline (PBS). Sections were then incubated with 5% normal horse serum for 20 minutes at 37°C, followed by incubation with the appropriate primary antibody for 1 hour. The following primary antibodies were used: a monoclonal mouse anti–smooth muscle Actin (SMA, 1:200; DakoCytomation, Carpinteria, CA), a mouse monoclonal anti-myosin (myosin heavy chain, clone hSM-V, 1:1000; Sigma-Aldrich, St. Louis, MO), a mouse monoclonal antidesmin (clone DE-U-10, 1:150; Sigma), a mouse monoclonal antivimentin (Clone LN-6, 1:200, Sigma), and a mouse monoclonal anti-CD31(1:30; Dako). After the primary antibody incubation, slides were rinsed in PBS and incubated with biotinylated secondary horse antimouse IgG (Vector Laboratories) at 37°C for 1 hour, they were stained with diaminobenzidine-tetrahydrochloride substrate kit (Vector Laboratories) for horseradish peroxidase followed by counter stain with Gill hematoxylin (Sigma Diagnostics). Positive controls included human tissues that were positive for SMA, myosin, desmin, vimentin, and CD31. Negative controls were performed with nonimmune normal serum used instead of the primary antibody.

Immunofluorescence

The slides were deparaffinized and hydrated in distilled water and then microwave pretreated as for IHC. The slides were incubated with 4% normal donkey serum in Tris buffered saline (TBS) buffer for 20 minutes at 37°C, followed by incubation with primary antibodies SMA (mouse monoclonal antibody, 1:200; Dako) and vimentin (goat monoclonal antibody, 1:40; Sigma) in TBS buffer for 1 hour at 37°C, then 4°C overnight. Positive and negative controls were used as above. After incubation, the sections were rinsed in TBS buffer, followed by incubation with secondary antibodies (Cy5 conjugated donkey antimouse IgG; fluorescein isothiocyanate (FITC)–conjugated donkey anti-goat IgG) for 2 hours at room temperature. Finally, the sections were rinsed in TBS and then dehydrated through alcohols, cleared in xylene, and mounted with EZ-Mount. The sections were viewed and imaged with a fluorescence confocal microscope. The negative control was the same as described above.

Results

Human Cerebral Aneurysm

Gross examination showed an aneurysm filled with coils at the junction of the vertebral and basilar arteries. Coils within the aneurysm were visible through the thin, translucent aneurysm wall. The neck of the aneurysm was completely covered by thin, translucent smooth membranous tissue (Fig 1*A*). The measured aneurysm size was $10 \times 8 \times 9$ mm (length $\times$ width $\times$ height) and the neck size was 4×8 mm (length $\times$ width).

Light-microscopic evaluation of the H&E stained slides showed a hypocellular, faintly stained, amorphous tissue that filled most aneurysm cavity (Fig 1*B*). Scattered, chronic inflammatory cells and thin-walled neovessels were noted in the dome. Poorly organized thrombus occupied portions of the cavity (Fig 1*C*),

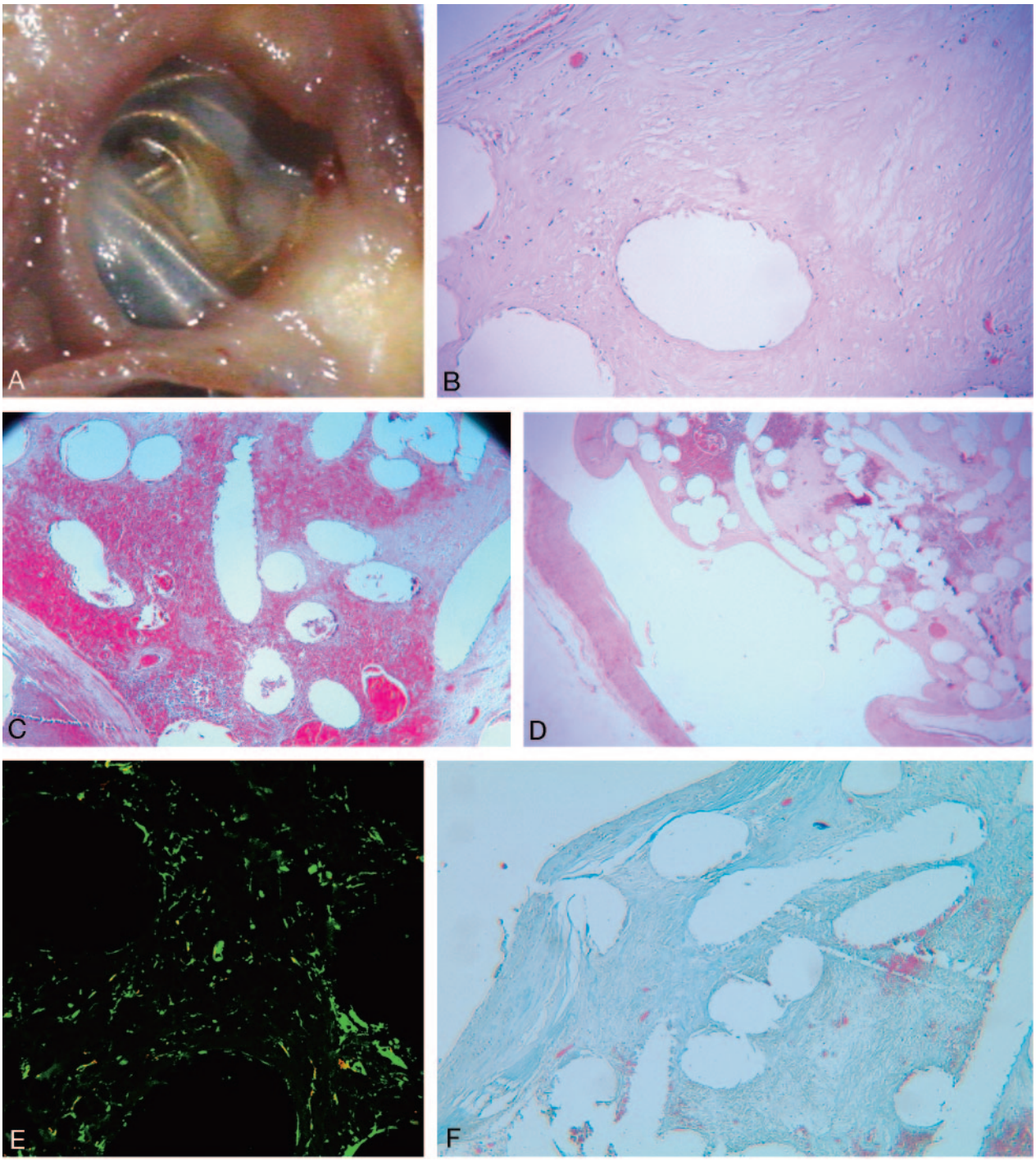

FIG 1. Human vertebrobasilar aneurysm embolized with platinum coils.

A, Gross photograph showing thin membranous tissue at the neck with coil loops that are visible through the membrane.

B, Section of the vertebrobasilar aneurysm stained with H&E (magnification 100×). The photomicrograph shows hypocellular, amorphous tissue in the dome.

C, Section of the aneurysm stained with H&E (magnification 60×). This photomicrograph shows a large area of poorly organized thrombus in the aneurysm dome.

D, Section stained with H&E (magnification 20×). A photomicrograph showing a thin layer of hypocellular tissue covering the neck of aneurysm.

E, Immunofluorescent double stain of the vertebrobasilar aneurysm, with antibodies for SMA (*red*) and vimentin (*green*) (magnification 20×; oil). This photomicrograph shows scattered, sparse cells within the aneurysm dome, which are positive for vimentin, but negative for SMA.

F, Stained with Masson trichrome (magnification 60×). It reveals that collagen deposition was absent in the aneurysm.

accompanied by localized, chronic inflammatory infiltrates. A thin layer of hypocellular tissue, lined with a single layer of flattened CD31-positive endothelial cells, bridged the entire neck (Fig 1*D*). The tissue

covering the neck became thicker near the junction with the parent artery. SMA and vimentin double immunofluorescent staining showed most sparse cells within dome were positive for vimentin and negative for SMA (Fig 1*E*), which indicates that these cells were fibrocytes and inflammatory cells. Collagen deposition was absent within the dome and along the neck (Fig 1*F*).

Rabbit Aneurysms

Gross examination displayed that 5 of 6 samples showed the neck orifice of aneurysm partially or completely was covered with thin, translucent membranous tissue (Fig 2*A*). One aneurysm demonstrated no membranous tissue covering.

Light microscopy showed hypocellular, loose, cotton-like, faintly stained tissue (Fig 2*B*) filling the dome in all 6 aneurysms. This tissue was associated with thin-walled neovessels and occasional giant cells. One sample showed small areas of residual, poorly organized thrombus in the dome. Three of 6 aneurysms had scattered chronic inflammation foci surrounding some coil winds or within the loose tissue. Thin layers of hypocellular tissue bridged the aneurysm neck in 5 of 6 samples (Fig 2*C*), which were lined with a single layer of CD31-positive endothelial cells. Tissue bridging the neck was concave to the aneurysm cavity and became thicker and more cellular near the junction with the parent artery. One aneurysm showed unorganized fibrin mixed with red blood cells along the interface between the cavity and parent artery, which was concave to the aneurysm cavity. Collagen deposition was not present in any of the rabbit aneurysm domes, as evidenced by Masson trichrome staining (Fig 2*D*).

IHC showed most the cells within the lumen were negative for SMA, myosin, and desmin. Double immunofluorescent staining for vimentin and SMA revealed that most round cells as well as the thin, shortened spindle cells within the dome were positive for vimentin but negative for SMA. The presence of vimentin in the absence of SMA indicated that the cells were fibrocytes or inflammatory cells (Fig 2*E*).

Swine Aneurysms

Gross examination demonstrated that all 5 swine aneurysms were completely covered with thick, smooth, white membranous tissue, which entirely separated the aneurysm from the parent artery (Fig 3*A*). An examination of the specimens with light microscopy revealed that 2 of 5 specimen lumens were mainly filled with chronic inflammatory tissue; consisting of lymphocytes, histocytes, macrophages, and thin-walled vessels (Fig 3*B*). Localized collagen deposition surrounding the thin-walled vessels was identified. Three of 5 samples demonstrated the aneurysm dome to be occupied with highly vascularized fibrous tissue (Fig 3*C*). Masson trichrome stain showed abundant, attenuated, collagen fiber bundles surrounding the vessels or coil winds throughout the entire dome (Fig 3*D*). These fiber bundles were associated with rich, elongated spindle cells. Two of these 3 samples had several foci of markedly attenuated chronic inflammatory cell infiltration, consisting of lymphocytes and histiocytes. A thick layer, approximately 1 mm, of hypercellular, attenuated tissue bridged the entire aneurysm neck and completely separated the aneurysms from the parent artery in all 5 aneurysms (Fig 3*E*). This thick, hypercellular tissue consisted of 3 identifiable layers. The most superficial layer had endothelial cells continuous with that of the parent artery. The middle layer consisted of abundant, plump, elongated spindle cells. In the deepest layer, loosely packed, thin spindle cells were embedded in abundant collagen matrix. IHC and IF showed positive staining for SMA, desmin, myosin, and vimentin (Fig 3*F*), which indicated a myofibroblastic lineage that is typical for neointimal hyperplasia.

Discussion

In the current study, a modified histologic technique for paraffin embedding, sectioning, and staining of coil-embolized aneurysms was used. This tissue-processing technique permitted the application of numerous histologic stains, including immunohistochemical, immunofluorescent, and other special stains, not routinely employed, for direct comparison of rabbit, swine, and human histology. These data indicate that, in the long term, platinum coil embolization of human cerebral aneurysms yields a hypocellular, loose tissue meshwork in the dome, associated with a thin membrane covering the neck. Collagen deposition and infiltration by contractile cells were absent. Experimental rabbit aneurysms also had a hypocellular matrix in the dome, thin neck coverage, and the absence of collagen deposition and contractile cells. Conversely, swine aneurysms showed thick neointimal formation, attenuated tissue infiltration, and robust collagen deposition. These data confirm that in both rabbit and human aneurysms platinum coils fail to induce fibrosis and cellular proliferation while swine aneurysms undergo robust collagen scar formation after treatment with platinum coils.

The findings in our single human case are similar to those seen in previous reports (5, 6). Relatively wide necked aneurysms in humans may retain unorganized thrombus for prolonged durations (2–4). Further, neck coverage tends to remain thin, irrespective of neck size. Our data provide further insights on healing in human aneurysms, not previously reported, by using IHC and immunofluorescent staining. Previous reports have suggested the presence of endothelial cell coverage on the basis of scanning electron microscopy (5). Our study confirms, through the use of IHC, that the cells lining the neck are indeed CD-31-positive endothelial cells. Multiple previous reports have suggested the presence of fibrocytes in the dome (5, 6, 38). The application of multiple antibodies demonstrates that spindle cells in the aneurysm dome are fibrocytes and not contractile cells such as smooth muscle cells or myofibroblasts. Finally, Masson trichrome staining, which had not previously been

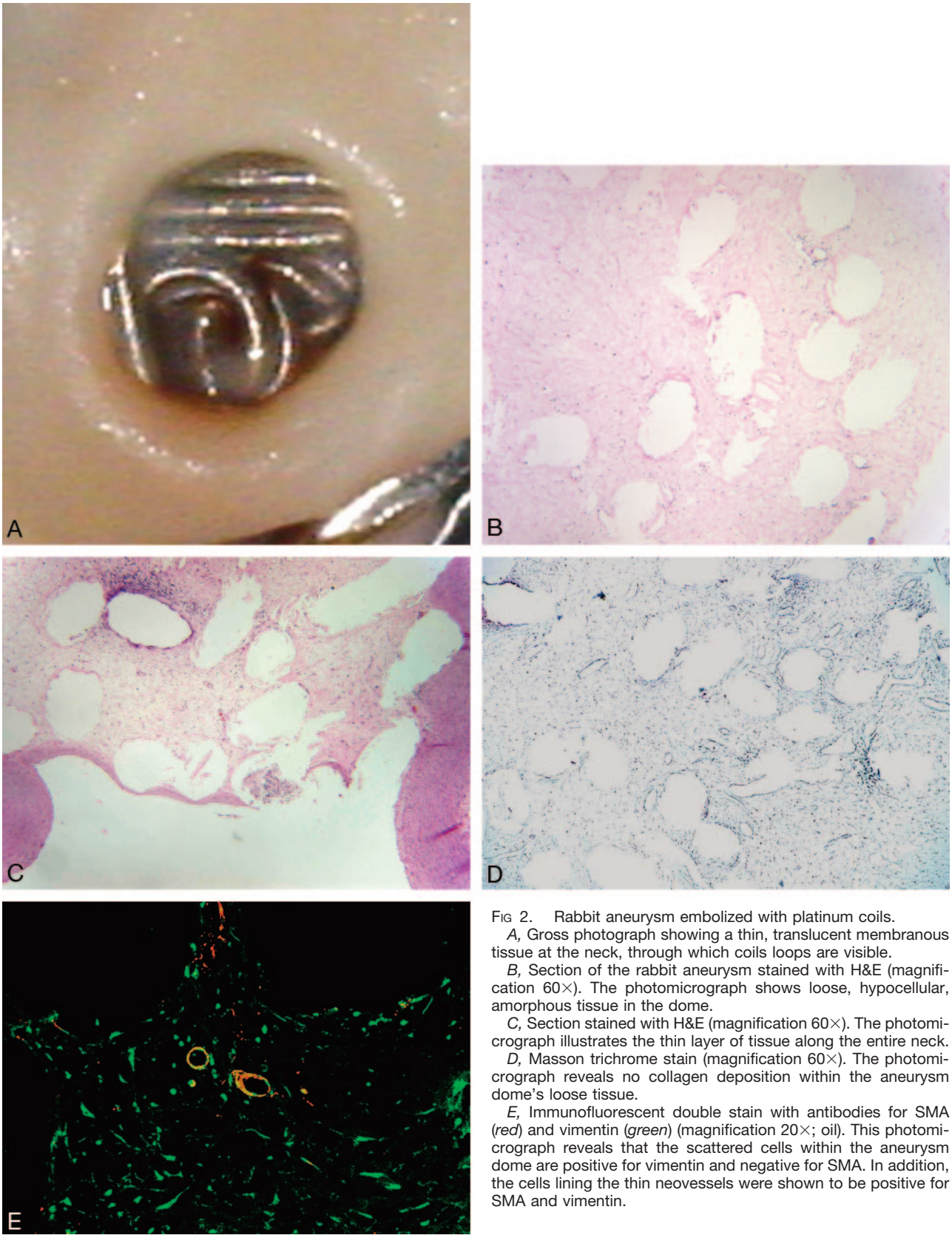

FIG 2. Rabbit aneurysm embolized with platinum coils.

A, Gross photograph showing a thin, translucent membranous tissue at the neck, through which coils loops are visible.

B, Section of the rabbit aneurysm stained with H&E (magnification 60×). The photomicrograph shows loose, hypocellular, amorphous tissue in the dome.

C, Section stained with H&E (magnification 60×). The photomicrograph illustrates the thin layer of tissue along the entire neck.

D, Masson trichrome stain (magnification 60×). The photomicrograph reveals no collagen deposition within the aneurysm dome's loose tissue.

E, Immunofluorescent double stain with antibodies for SMA (*red*) and vimentin (*green*) (magnification 20×; oil). This photomicrograph reveals that the scattered cells within the aneurysm dome are positive for vimentin and negative for SMA. In addition, the cells lining the thin neovessels were shown to be positive for SMA and vimentin.

applied to human aneurysm tissue after coiling, showed that there is near absence of collagenous matrix.

Previous studies in rabbits have neither directly compared these experimental aneurysms to human aneurysms nor applied special stains to the aneurysm

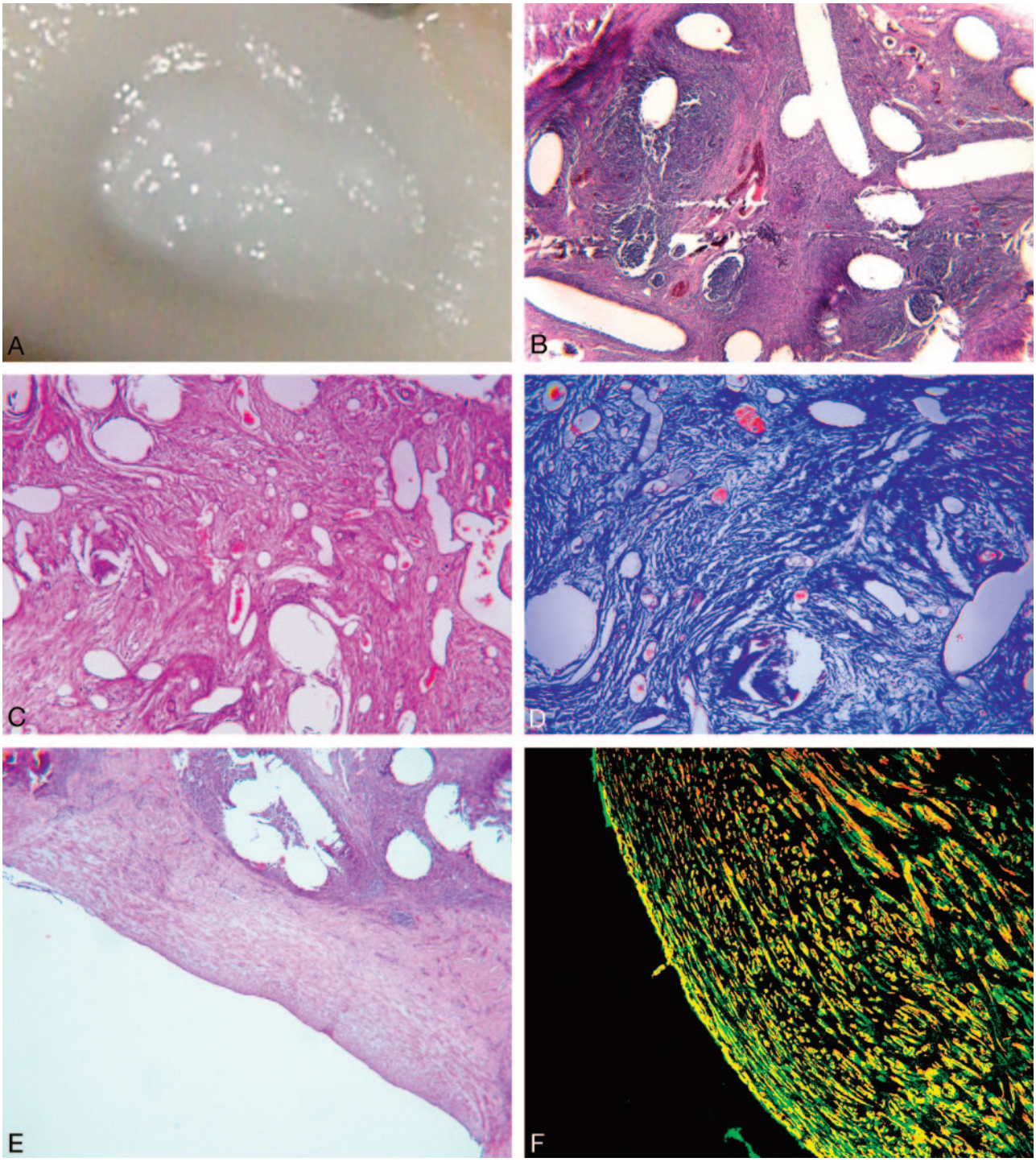

FIG 3. Swine aneurysm embolized with platinum coils.

A, Gross photograph showing a smooth, thick membrane completely covering the neck. Coil loops are not visible through this membrane.

B, Section of the swine aneurysm stained with H&E (magnification 60×). The photomicrograph shows diffuse, attenuated chronic inflammatory tissue within the aneurysm dome.

C, Stained with H&E (magnification 60×). This photomicrograph shows extensive, attenuated, fibrous tissue within the dome, which is associated with rich neovessels.

D, Section stained with Masson trichrome (magnification 60×). A photomicrograph shows diffuse, attenuated, abundant, collagen fibers within the aneurysm dome.

E, Section stained with H&E (magnification 40×). A photomicrograph of this stained section shows a thick layer of hypercellular tissue along aneurysm neck.

F, Immunofluorescent double stain with antibodies for SMA (*red*) and vimentin (*green*) (magnification = 20×; oil). This photomicrograph reveals the attenuated cells at neck of aneurysm are positive for both SMA and vimentin, which indicates classic neointimal formation.

tissue. Terms, such as spindle-like cells, smooth muscle cell–like or endothelial-like cells have been used to describe the cells involved in the healing process after coil embolization. Scarlike tissue and fibrous tissue have been employed to describe the tissue reaction, without giving the details of the matrix. The exact cell or tissue types were never identified in these reports. Our findings, which employ light microscopy in rabbit aneurysms, are in general agreement with prior studies (8, 9, 11) and indicate relatively poor overall healing. The current study confirms that the dome is filled with a loose, noncollagenous matrix populated by sparse fibrocytes. Neck healing is relatively poor, without substantial amounts of neointimal formation.

Data from the current study indicate that the key cell of extracellular matrix production, the myofibroblast, and the primary component of extracellular matrix, Type 1 collagen, are absent in the rabbit model and in one sample of a human aneurysm in the chronic phase after embolization. In contrast to rabbit aneurysms, the swine aneurysms demonstrated robust myofibroblast infiltration along the neck and attenuated collagen matrix deposition in the dome. As in previous reports, the data presented here suggest the cellular response to platinum coil embolization in the rabbit aneurysms was more similar to that reported in humans than was that of the swine aneurysms. The current study, combined with our previous studies (29, 30, 31), leads us to believe that elastase-induced aneurysms in the rabbit represent a valid model for the testing of endovascular devices.

Large animal models, including surgically created canine and swine models, have been extensively used for preclinical testing of endovascular devices (7, 12, 16–19, 24–28). Although model aneurysms in canines demonstrated high rates of patency if untreated (25, 26, 39), the aneurysm wall of these models are vein grafts that differ histologically from human saccular aneurysms. The hemodynamics of these sidewall models do not resemble those found in human aneurysms (40). In addition, a previous report (28) has demonstrated that, in a canine model, a thick layer of endothelialized neointima forms along the aneurysm neck, unlike findings seen in humans.

Disparity among species regarding the healing response to implanted devices is well known (41). Indeed, swine are used preferentially in testing coronary stents, because they are known to mount impressive neointimal proliferation in response to arterial implants (42). In the setting of aneurysm occlusion devices, a robust healing response, beyond that expected in humans, is suboptimal. That is, preclinical testing models that heal too easily would be unable to discern whether a certain device modification would necessarily improve healing in humans.

The ideal model for testing endovascular devices for aneurysm treatment would encompass all relevant aspects that might predict performance in humans. These attributes would include (1) clotting and thrombolytic systems similar to humans; (2) hemodynamic similarity to intracranial aneurysm and parent artery morphology in humans; (3) immunologic response similar to humans; and (4) tissue reaction similar to humans. The rabbit elastase model offers hemodynamic and morphologic similarity to humans and likely mimics the tissue response. Swine have been proposed as a relevant model because of similarity in the coagulation system between swine and humans (7, 17–19). Further, swine xenografts have been proposed for transplantation into humans (43–45). We believe, however, that coagulation and immunologic similarities are substantially less relevant than hemodynamic and healing considerations when choosing a preclinical model for testing aneurysm devices.

This study, though offering important insight into the healing of experimental aneurysms, has some shortcomings. Only a single human sample was available for review. We currently are attempting to increase the number of human samples through advertising in pathology journals but, thus far, have failed to secure additional samples. In addition, we chose a single time point for implantation in rabbits of 24 weeks and in swine of 12 weeks. Longer duration of implantation in swine yields animals too large to fit on an angiography table. It is highly likely that longer implant duration in swine would not change the healing, which was essentially complete at 12 weeks. In rabbits, we have observed that healing tends to plateau at 12–18 weeks (authors' unpublished data). Thus, we can assume that healing is also likely complete in the rabbit aneurysms included in this study.

Conclusions

Absence of collagen deposition and scant myofibroblastic reaction to platinum coil embolization are seen in rabbit models but not in swine aneurysms. The elastase-induced aneurysm model in rabbits is more suitable than sidewall swine aneurysms for testing of modified devices aimed at improving intra-aneurysmal fibrosis.

Acknowledgments

We wish to express our gratitude to Dr. Robert Macaulay, Department of Pathology and Laboratory Medicine, Queen Elizabeth II Health Sciences Centre, Halifax, Nova Scotia, for his generous help with the study.

References

1. Castro E, Fortea F, Villoria F, et al. **Long-term histopathologic findings in two cerebral aneurysms embolized with Guglielmi detachable coils.** *AJNR Am J Neuroradiol* 1999;20:549–552
2. Molyneux A, Ellison D, Morris J, Byrne J. **Histological findings in giant aneurysms treated with Guglielmi detachable coils: report of two cases with autopsy correlation.** *J Neurosurg* 1995;83:129–132
3. Shimizu S, Kurata A, Takano M, et al. **Tissue response of a small saccular aneurysm after incomplete occlusion with a Guglielmi detachable coil.** *AJNR Am J Neuroradiol* 1999;20:546–548
4. Mizoi K, Yoshimoto T, Takahashi A, Nagamine Y. **A pitfall in the surgery of a recurrent aneurysm after coil embolization and its histological observation: technical case report.** *J Neurosurg* 1996;39:165–168

5. Ishihara S, Mawad M, Ogata K, et al. **Histopathologic findings in human cerebral aneurysms embolized with platinum coils: report of two cases and review of the literature.** *AJNR Am J Neuroradiol* 2002;23:970–974
6. Groden C, Hagel C, Delling G, Zeumer H. **Histological findings in ruptured aneurysms treated with GDCs: six examples at varying times after treatment.** *AJNR Am J Neuroradiol* 2003;24:579–584
7. Murayama Y, Vinuela F, Suzuki Y, et al. **Ion implantation and protein coating of detachable coils for endovascular treatment of cerebral aneurysms: concepts and preliminary results in swine models.** *Neurosurgery* 1997;40:1233–1243
8. Reul J, Weis J, Spetzger U, et al. **Long-term angiographic and histopathologic findings in experimental aneurysms of the carotid bifurcation embolized with platinum and tungsten coils.** *AJNR Am J Neuroradiol* 1997;18:35–42
9. Kallmes DF, Helm GA, Hudson SB, et al. **Histologic evaluation of platinum coil embolization in an aneurysm model in rabbits.** *Radiology* 1999;213:217–222
10. Abrahams JM, Forman MS, Grady M, Diamond SL. **Biodegradable polyglycolide endovascular coils promote wall thickening and drug delivery in a rat aneurysm model.** *Neurosurgery* 2001;49:1187–1193
11. Bocher-Schwarz HG, Ringel K, Bohl J, et al. **Histological findings in coil-packed experimental aneurysms 3 months after embolization.** *Neurosurgery* 2002;50:379–384
12. Dawson RC, Krisht AF, Barrow DL, et al. **Treatment of experimental aneurysms using collagen-coated microcoils.** *Neurosurgery* 1995;36:133–139
13. Kallmes DF, Borland MK, Cloft HJ, et al. **In vitro proliferation and adhesion of basic fibroblast growth factor-producing fibroblasts on platinum coils.** *Radiology* 1998;206:237–243
14. Kallmes DF, Williams AD, Cloft HJ, et al. **Platinum coil-mediated implantation of growth factor-secreting endovascular tissue grafts: an in vivo study.** *Radiology* 1998;207:519–523
15. Kwan E, Heilman CB, Roth PA. **Endovascular packing of carotid bifurcation aneurysm with polyester fiber-coated platinum coils in a rabbit model.** *AJNR Am J Neuroradiol* 1993;14:323–333
16. Szikora I, Wakhloo AK, Guterman LR, et al. **Initial experience with collagen-filled Guglielmi detachable coils for endovascular treatment of experimental aneurysms.** *AJNR Am J Neuroradiol* 1997;18:667–672
17. Murayama Y, Suzuki Y, Vinuela F, et al. **Development of a biologically active Guglielmi detachable coil for the treatment of cerebral aneurysms. Part I. In vitro study.** *AJNR Am J Neuroradiol* 1999;20:1986–1991
18. Murayama Y, Vinuela F, Suzuki Y, et al. **Development of the biologically active Guglielmi detachable coil for the treatment of cerebral aneurysms. Part II. An experimental study in a swine aneurysm model.** *AJNR Am J Neuroradiol* 1999;20:1992–1999
19. Murayama Y, Tateshima S, Gonzalez NFV. **Matrix and bioabsorbable polymeric coils accelerate healing of intracranial aneurysms: long-term experimental study.** *Stroke* 2003;34:2031–2037
20. de Gast AN, Altes TA, Marx WF, et al. **Transforming growth factor beta-coated platinum coils for endovascular treatment of aneurysms: an animal study.** *Neurosurgery* 2001;49:690–694
21. Marx WF, Cloft HJ, Helm GA, et al. **Endovascular treatment of experimental aneurysms by use of biologically modified embolic devices: coil-mediated intraaneurysmal delivery of fibroblast tissue allografts.** *AJNR Am J Neuroradiol* 2001;22:323–333
22. Kallmes DF, Fujiwara NH, Yuen D, et al. **A collagen-based coil for embolization of saccular aneurysms in a New Zealand white rabbit model.** *AJNR Am J Neuroradiol* 2003;24:591–596
23. Kallmes D, Fujiwara N. **New expandable hydrogel-platinum coil hybrid device for aneurysm embolization.** *AJNR Am J Neuroradiol* 2002;23:1580–1588
24. Dawson RC III, Shengelaia GG, Krisht AF, Bonner GD. **Histologic effects of collagen-filled interlocking detachable coils in the ablation of experimental aneurysms in swine.** *AJNR Am J Neuroradiol* 1996;17:853–858
25. Graves VB, Partington CR, Rufenacht DA, et al. **Treatment of carotid artery aneurysms with platinum coils: an experimental study in dogs.** *AJNR Am J Neuroradiol* 1990;11:249–252
26. Graves VB, Strother CM, Partington CR, Rappe A. **Flow dynamics of lateral carotid artery aneurysms and their effects on coils and balloons: an experimental study in dogs.** *AJNR Am J Neuroradiol* 1992;13:189–196
27. Graves VB, Strother CM, Rappe AH. **Treatment of experimental canine carotid aneurysms with platinum coils.** *AJNR Am J Neuroradiol* 1993;14:787–793
28. Mawad ME, Mawad JK, Cartwright JR, Gokaslan Z. **Long-term histopathologic changes in canine aneurysms embolized with Guglielmi detachable coils.** *AJNR Am J Neuroradiol* 1995;16:7–13
29. Altes TA, Cloft HJ, Short JG, et al. **Creation of saccular aneurysms in the rabbit: a model suitable for testing endovascular devices.** *AJR Am J Roentgenol* 2000;174:349–354
30. Short JG, Fujiwara NH, Marx WF, et al. **Elastase-induced saccular aneurysms in rabbits: comparison of geometric features with those of human aneurysms.** *AJNR Am J Neuroradiol* 2001;22:1833–1837
31. Fujiwara NH, Cloft HJ, Marx WF, et al. **Serial angiography in an elastase-induced aneurysm model in rabbits: evidence for progressive aneurysm enlargement after creation.** *AJNR Am J Neuroradiol* 2001;22:698–703
32. Fujiwara NH, Kallmes DF. **Healing response in elastase-induced rabbit aneurysms after embolization with a new platinum coil system.** *AJNR Am J Neuroradiol* 2002;23:1137–1144
33. Kerber CW, Heilman CB. **Flow dynamics in the human carotid artery. I. Preliminary observations using a transparent elastic model.** *AJNR Am J Neuroradiol* 1992;13:173–180
34. Kerber CW, Liepsch D. **Flow dynamics for radiologists. II. Practical considerations in the live human.** *AJNR Am J Neuroradiol* 1994;15:1076–1086
35. Kondo S, Hashimoto N, Kikuchi H, et al. **Cerebral aneurysms arising at nonbranching sites: an experimental study.** *Stroke* 1997;28:398–403
36. Sekhar LN, Heros RC. **Origin, growth, and rupture of saccular aneurysms: a review.** *Neurosurgery* 1981;8:248–260
37. German W, Black S. **Experimental production of carotid aneurysms.** *N Engl J Med* 1954;3:463–468
38. Bavinzski G, Talazoglu V, Killer M, et al. **Gross and microscopic histopathological findings in aneurysms of the human brain treated with Guglielmi detachable coils.** *J Neurosurg* 1999;91:284–293
39. Kallmes DF, Altes TA, Vincent DA, et al. **Experimental side-wall aneurysms: a natural history study.** *Neuroradiology* 1999;41:338–341
40. Strother CM, Graves VB, Rappe A. **Aneurysm hemodynamics: an experimental study.** *AJNR Am J Neuroradiol* 1992;13:1089–1095
41. Carter A, Laird J, Farb A, et al. **Morphologic characteristics of lesion formation and time course of smooth muscle cell proliferation in a porcine proliferative restenosis model.** *J Am Coll Cardiol* 1994;24:1398–1405
42. Kantor B, Ashai K, Holmes DJ, Schwartz R. **The experimental animal models for assessing treatment of restenosis.** *Cardiovasc Radiat Med* 1999;1:48–54
43. Brenner P, Reichenspurner H, Schmoeckel M, et al. **Ig-therasorb immunoapheresis in orthotopic xenotransplantation of baboons with landrace pig hearts.** *Transplantation* 2000;39:208–214
44. Cooper D. **Clinical xenotransplantion: how close are we?** *Lancet* 2003;362:557–559
45. McGregor C, Teotia S, Byrne G, et al. **Cardiac xenotransplantation: progress toward the clinic.** *Transplantation* 2004;78:1569–1575